# Optimal rolling manoeuvres with very flexible wings

Salvatore Maraniello* and Rafael Palacios†

*Imperial College, London, SW7 2AZ, United Kingdom*

**The single-shooting method is used to identify optimal manoeuvres in the lateral dynamics of partially-supported flexible wings. Efficient actuation strategies are sought when large wing deflections substantially modify the geometry of the vehicle during the manoeuvre. For that purpose, geometrical nonlinear models are first built using composite beams and an unsteady vortex lattice, and the optimal control problem is then solved via a gradient-based algorithm. A flight-dynamics model based on elastified stability derivatives is shown to capture the relevant dynamics either under slow actuation or for stiff wings and it is used as a reference. Embedding the full aeroelastic description into the optimisation framework expands the space of achievable manoeuvres, such as quick wing response with low structural vibrations or large lateral forces with minimal lift losses.**

## Nomenclature

| | |
|---|---|
| $\alpha$ | Angle of attack measured at the wing root chord |
| $\beta$ | Aileron deflection angle |
| $\eta$ | Vector containing wing nodal displacements and rotations |
| $\Phi$ | Wing roll angle |
| $\psi$ | Basis function used to parametrise the control time history |
| $\sigma$ | Wing stiffness parameter |
| $A$ | Body-attached frame of reference |
| $B$ | Local frame of reference defined along the beam mean axis $s$ |

*Graduate Student, Department of Aeronautics

†Reader, Department of Aeronautics, 355 Roderic Hill Building; r.palacios@imperial.ac.uk. AIAA Member.

| | |
|---|---|
| $b$ | Wing span length |
| $C$ | Column vector for the optimisation problems constrains |
| $c$ | Wing chord length |
| $C_{M_p}$ | Stability/control derivatives of aerodynamic moment with respect to the generic parameter $p$ |
| $F_T$ | Target lateral force used to define lateral manoeuvres |
| $F_Y$ | Aerodynamic lateral force measured in the global frame of reference G |
| $F_Z$ | Aerodynamic vertical force measured in the global frame of reference G |
| $G$ | Inertial frame of reference |
| $I$ | Cost function for the optimisation problems |
| $I_{xx}$ | Wing rotatory inertia about $x$ axis of FoR A |
| $L$ | Lift force in steady level flight |
| $M_a$ | Moment produced by aerodynamics forces |
| $M_g$ | Moment produced by gravity |
| $R$ | Position of the local frame $B$ with respect to the body frame $A$ |
| $s$ | Beam mean axis |
| $T$ | Final time of the dynamic simulations |
| $t$ | Time |
| $u$ | Control function |
| $U_\infty$ | Free stream velocity |
| $x$ | Column vector containing the design variables for the optimisation problems |
| $y$ | Physical system state |

---

| | |
|---|---|
| EFDM | Elastified flight dynamics model |
| FoR | Frame of reference |
| GEBM | Geometrically-exact beam model |
| UVLM | Unsteady vortex-lattice method |

# I. Introduction

Aircraft design has long been characterised by relatively stiff wings exhibiting small structural deformations and frequency separation between flight-dynamics and structural modes. For this reason, flexible vehicle flight simulation often relies on the use of *elastified* stability derivatives, typically obtained by correcting the

rigid aircraft stability derivatives with flex-to-rigid ratios provided by a linear aeroelastic analysis.[1–3] For loads prediction and flight control development, these equations can be augmented with the low-frequency dynamics of the structure. When deflections are small, perturbation on the structural degrees of freedom allows solving the coupled rigid/flexible body dynamics using a few aeroelastic modes.[4–8]

As wings with higher aspect ratio and flexibility are considered, the coupling between the rigid body dynamics and the nonlinear aeroelastic response becomes increasing relevant. Assessing the manoeuvrability and controllability of very flexible vehicles requires, therefore, an adjustment of classical linear approaches for control and flight simulation. A typical solution for stability and flutter analysis consists on linearising the aeroelastic system around a fixed trimmed configuration[8–10]. While this allows to capture the effect of the geometry changes at different trim points, the linearisation needs to be repeated for each point of the flight envelope. Large geometric changes may occur however not only within different points of the flight envelope but also within a single manoeuvre, and consequently a number of fully coupled simulation strategies, based on geometrically-nonlinear descriptions of the wing structural model, have been developed.[11–13]

Control synthesis can benefit from this nonlinear aeroelastic description of the very flexible aircraft dynamics, although to date the proposed control strategies are still based on linear methods.[14–16] Importantly, this does not only apply to the development of feedback control laws (e.g. for trajectory tracking and disturbance rejection), but also when the objective is to to determine efficient (open-loop) strategies for manoeuvring. Indeed, the additional knowledge gained by nonlinear characterisation of the flexible vehicle dynamics can also provide new opportunities to identify nominal manoeuvres that give extra performance. The task of identifying such manoeuvres can be addressed by solving an optimal control problem with respect to the time histories of the aerodynamic control surfaces. To make this computationally-tractable, the control input needs to be parametrised and a solution can be found numerically via nonlinear programming techniques for optimisation (direct methods). As the coefficients of the parametrisation become design parameters handled directly by the optimisation algorithm, there is a strong link between direct methods for optimal control and multidisciplinary optimisation architectures (MDO).[17;18]

In direct transcription (DT) deriving methodologies, both state and control are discretised in time and treated as design variables. From a MDO point of view, this corresponds to an all-at-once architecture, in which physical solution and optimal control are found simultaneously. While DT deriving methods can explore infeasible and unstable states, thus possibly leading to a faster convergence of the optimisation, the number of design variables is drastically increased. In single shooting, or control vector parametrisation, which will be the approach followed in this work, the problem is therefore recast into a multidisciplinary

feasible architecture: only the coefficients of the control input parametrisation are treated as design parameters and at each iteration of the optimisation the state of the system is determined through an aeroelastic analysis. This approach reduces the design space size and offers the advantage of an easy implementation, as pre-existing aeroelastic solvers can be used; on the other hand, only feasible states are explored and more iterations may be required to terminate the optimisation. A previous study has already shown how the single-shooting method can be used to achieve optimal dynamic performance of very flexible slender structures, even when they exhibit a highly nonlinear behaviour.[19]

In this work an optimisation framework has been built around an aeroelastic simulation environment for very flexible aircraft (Sec. II). The dynamics of the primary structures are described using geometrically-exact beam equations (GEBM), which are discretised using finite elements and solved with respect to a moving reference frame[20;21]. The will be assumed to be lifting surfaces undergoing arbitrary kinematics at low speeds, whose aerodynamics will be given by the unsteady vortex-lattice method (UVLM).[8;22;23] In order to assess the importance of nonlinear effects in the full solution, a lower-fidelity flight-dynamics model, based on elastified stability derivatives,[2;3] has also been derived (Sec. II.C and III.C). Focusing on rolling manoeuvres, in Sec. III.A and III.B both descriptions are used to assess key manoeuvrability features of vehicles with very flexible wings and the relative importance of geometrically-nonlinear effects. To this aim, simulation models of high-aspect ratio wings in hinged configuration have been built. The hinge constraint allows to isolate the dynamics associated to the wing from that of the rest of the aircraft. Control is exerted through a single aileron on each wing at a predefined location, although the present approach can be directly extended to more complex actuator layouts, for instance, to generate additional wing twisting[24], or include parametrisations of actuator location. The full aeroelastic implementation is assessed against the results obtained through the flight-dynamics description and used to investigate the trade-off between some relevant performance indices — namely quick response against low structural vibrations and gain in lateral force against lift loss — associated to rolling manoeuvres.

## II. Methodology

This section introduces first the chosen framework for flexible vehicle dynamics modelling, whose implementation has been extensively verified in previous studies.[8;25;26] (Sec. II.A). The integration of the nonlinear aeroelastic solution into a single shooting based framework for optimal control is then discussed in Sec. II.B. Finally, Sec. II.C introduces elastified stability derivatives to estimate the impact of aeroelastic effects on the roll dynamics.

### II.A. Aeroelastic Model

The coupled flexible-rigid body dynamic structural model is described using the frames of reference (FoRs) ashown in Fig. 1. The rigid-body dynamics is expressed in terms of translational ($v_A$) and angular ($\omega_A$) velocity vectors of a FoR attached to the body, $A$, with respect to the inertial frame $G$. A linear elastic material behaviour is assumed. At each section of the beam, force and moment strains are expressed into a local frame $B$, defined along the beam mean axis, with curvilinear coordinate $s$.[20] Its position is given by the vector $R$, while the orientation is expressed using a Cartesian rotation vector. As the $B$ frame can freely move and rotate with respect to the body attached frame, $A$, large displacements and rotations are accurately captured. The structures are discretised using quadratic finite elements, and as a result the coupled nonlinear flexible-rigid body dynamics is expressed as

$$M(\eta)\begin{Bmatrix} \ddot{\eta} \\ \dot{\chi} \end{Bmatrix} + \begin{Bmatrix} Q^s_{gyr}(\eta,\dot{\eta},\chi) \\ Q^r_{gyr}(\eta,\dot{\eta},\chi) \end{Bmatrix} + \begin{Bmatrix} Q^s_{stif}(\eta) \\ 0 \end{Bmatrix} = \begin{Bmatrix} Q^s_{ext}(\eta,\dot{\eta},\zeta,t) \\ Q^r_{ext}(\eta,\dot{\eta},\zeta,t) \end{Bmatrix} \tag{1}$$

where $\chi^T = \left\{v_A^T, \omega_A^T\right\}$, $\eta$ is a vector containing nodal rotation and displacements, and $Q_{gyr}$, $Q_{stiff}$, $Q_{ext}$ are, respectively, gyroscopic, stiffness and external forcing terms.[8] The external force $Q_{ext}$ includes both gravitational and aerodynamic contributions. The discrete mass matrix, $M$, includes the tangent operator to differentiate the rotation vector and consequently depends on the rotational degrees of freedom. The orientation of the body frame, $A$, is expressed through quaternions, $\zeta$, and is obtained through integration of the rigid-body angular velocity, $\omega_A$. Finally, hinge boundary conditions have been implemented to restrict the kinematics to only rotations about one axis.

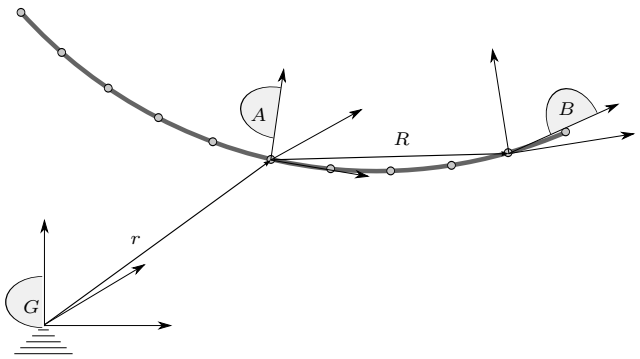



Figure 1: Definition of frames of reference

The aerodynamic component of the external forcing term, $Q_{ext}$, is computed via the UVLM, for which a detailed description is provided by Murua et al.[22] This assumes an incompressible potential flow, which is a realistic assumption for low Mach numbers, fully attached, flows. The no separation hypothesis implies that changes in wing geometry occur slowly with respect to the flow characteristic time scales. Under these conditions, a discretisation in vortex rings can be introduced on the aerodynamic surfaces and their wakes. The movement of the control surfaces is approximated by deflecting the corresponding wing panels.

Being $\Gamma$ the circulation strength associated to each of them, the velocity induced by a single vortex is computed using the Biot-Savart law and the global velocity field is derived through superposition. At each time step, vorticity is shed at the trailing edge, thus building up the wake. To capture the effect of large deflections, in particular, the wake geometry is computed as part of the solution by convecting the vortex rings according to the free-stream flow velocity. The vorticity field at the time-step $n$ is solved by enforcing the non-penetration condition at a number of collocation points distributed over the wing, thus leading to:

$$A_b(\eta)\Gamma_b^n + A_w(\eta)\Gamma_w^n + w^n(\eta, \dot{\eta}, \chi, \zeta) = 0 \tag{2}$$

In eq. (2) $\Gamma_b$ and $\Gamma_w$ are the surface (bound) and wave strength circulation vectors, while $A_b$ and $A_w$ are the wing-wing and wing-wake aerodynamics influence coefficients matrices. These are updated at each time-step to account for geometrical changes. The first two terms in eq. (2) return the velocity induced by the vortex rings system at the collocation points, while the vector $w$ contains the normal velocity of the collocation points due to wing vibrations and rigid body motion, the movement of aerodynamic control surfaces and gust induced velocity. This term determines the coupling with the structural and control disciplines. Once the vorticity has been solved for, the global velocity field can be computed and used to derive the aerodynamic loads by means of Joukowski's theorem,[23] thus closing the coupling between structure and aerodynamics.

### II.B. Optimal Manoeuvres via Single Shooting

The optimal control will be defined as an optimisation problem in which the design variable is a time-dependent function, the control input $u(t)$. When using the single-shooting method, the aeroelastic analysis is solved at each iteration over a certain time horizon $[0, T]$ so as to determine the state vector,

$y = \{\eta, \chi, \zeta, \Gamma_b, \Gamma_w\}^T$. The problem takes, thus, the form

$$\begin{aligned} \text{min.} \quad & I = I\left(u, y(u), \dot{y}(u)\right) \\ \text{w.r.t.} \quad & u(t) \\ \text{s.t.} \quad & C(u, y(u)) \geq 0 \end{aligned} \tag{3}$$

where the dependency of the aeroelastic system state on the control input, $y = y(u)$, has been specified explicitly. In problem (3), $I$ is the cost functional to minimise while $C$ defines a set of design constraints. For the studies presented in this work the control input is always provided by the left and right wing aileron deflections, hence $u(t) = \{\beta_L(t), \beta_R(t)\}$. Realistic travel limits and a maximum rate of deflection are ensured by enforcing

$$\begin{aligned} &|\beta_*(t)| \leq \beta_{max} \\ &\qquad\qquad \text{for} \quad t \,\epsilon\, [0, T] \\ &|\dot{\beta}_*(t)| \leq \dot{\beta}_{max} \end{aligned} \tag{4}$$

A numerical solution to the infinite-dimensional optimisation problem (3) can be obtained by expressing the control signal, $u(t)$, as a linear combination of $N_c$ basis functions, $\psi_n(t)$,

$$u = \sum_{n=1}^{N_c} u_n \; \psi_n(t) \tag{5}$$

and minimising the cost, $I$, with respect to the coefficients of the parametrisation, $u_n$. In most optimal control problems, piecewise constant parametrisations are used.[27] However, to describe the movement of typical control actuators on a relatively large time domain, these would result in a very large number of design variables. While from a computational point of view adjoint methods work efficiently in this scenario, these present the additional development cost of building the adjoint model itself.

With the purpose of modelling smooth actuation signals while limiting the number of coefficients used to parametrise the control, $N_c$, only $\mathcal{C}^1$ continuous or higher parametrisations were considered for this work. In particular, B-splines have been chosen as they were seen to provide good convergence properties when integrated in a shooting based optimisation framework.[19] Given a set of $N_\tau$ control points $\tau_n$, a set of

$N_c = N_\tau + p - 1$ B-splines basis of order $p$ can be built recursively as[28]

$$\psi_n^{(0)}(t) = \begin{cases} 1 & \text{if } \tau_n < t < \tau_{n+1} \\ 0 & \text{else} \end{cases} \tag{6}$$

and

$$\psi_n^{(p)}(t) = \frac{t - \tau_n}{\tau_{n+p} - \tau_n}\psi_n^{(p-1)}(t) + \frac{\tau_{n+p+1} - t}{\tau_{n+p+1} - \tau_{n+1}}\psi_{n+1}^{(p-1)}(t) \quad , \quad p > 0 \tag{7}$$

Note that the frequency range of actuation can be estimated through Nyquist criterion. Hence, in order to capture a maximum frequency $f_{max}$, a spacing between control points $\Delta\tau \leq 1/2f_{max}$ is necessary. As the distance betwen control points dismishes, higher rates in $\dot{u}$ adn $\ddot{u}$ can be reconstructed.

In line with previous works in optimal control[28;29] a quasi-Newton method, the sequential least-squares quadratic programming (SLSQP) algorithm,[30] has been used to solve the optimisation problem. The implementation is monolithic and finite differences are used for the gradient evaluation. In all the problems considered, cost and constraint functions, as well as design parameters, are scaled to achieve comparable orders of magnitude. If all the constraints are verified, the optimisation process is stopped when the relative change in cost and constrains is below a tolerance value of 0.1%.

### II.C. Roll Dynamics Using Elastified Stability Derivatives

To assess the influence of the geometrically-nonlinear effects in the aeroelastic model, a simplified description of the flexible-wing dynamics has also been developed using elastified stability derivatives.[2;3] This will be referred to as elastified flight-dynamics model (EFDM). As the studies presented in Sec. III are based on a hinged wing model, the EFDM will also only address the wing roll dynamics. The approach can be, however, similarly extended to include other rigid-body degrees of freedom.

As shown in Fig. 2, the attitude between the body attached FoR A is expressed with respect to the inertial frame G through the angles $(\Theta, \Phi)$ associated, respectively, to a pitch and roll rotation. The free stream velocity, $U_\infty$, is parallel to the $X$ axis of the G frame and the wing position is identified through the unit vectors $\hat{c}$ and $\hat{n}$, which are, respectively, tangent and perpendicular to its root chord. The wing is hinged so as to roll about the $x$ axis of body attached FoR A, while its pitch attitude is fixed. Note that in this set-up the free stream velocity has no side-slip. This would be accounted for by including yaw rotations, $\Psi$, to the velocity vector, thus retrieving a description based upon a triad $(\Theta, \Phi, \Psi)$ for the rotation between wind and body attached axes[31], however this is not considered here.

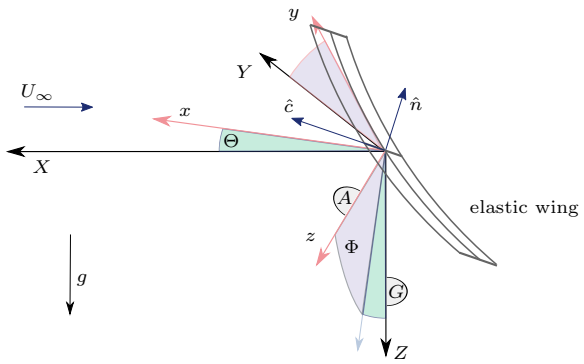



Figure 2: Definition of frames of references used for the flight-dynamics model

For a given free-stream dynamic pressure $q_\infty = 1/2\rho U_\infty^2$ (where $\rho$ is the air density), under the hinge kinematic constraint ($\dot{\Theta} = 0$) and neglecting structural dynamic effects ($\dot{\eta} = 0$), the wing roll dynamics is dictated by

$$I_{xx}(\eta(p))\ddot{\Phi} = M_{gx}(\Theta, \Phi, \eta(p)) + M_{ax}(\Theta, \Phi, \dot{\Phi}, \beta_L, \beta_R, \eta(p)) \tag{8}$$

where $M_{gx}$ and $M_{ax}$ are the $x$ components of the moments produced, respectively, by gravity and aerodynamic forces and $I_{xx}$ is the wing inertial about the $x$ axis. In general, all terms in eq. (8) will depend on the wing shape, defined here by the displacements and rotations, $\eta$, along the wing reference axis. The flying parameters determining these have been collected into the vector $p = (\Theta, \Phi, \dot{\Phi}, \beta_L, \beta_R)$.

Geometrically-nonlinear effects linked to gravity forces also need to be quantified. The exact location of the wing center of mass depends, in fact, on its deflections, hence a moment

$$M_{gx}(\Theta, \Phi, \eta) = g \cos\Theta \left[S_z(\eta) \sin\Phi - S_y(\eta) \cos\Phi\right] \tag{9}$$

where

$$S_i = \int_{-b/2}^{b/2} m \; R_{A_i}(s, \eta(p)) \; ds \tag{10}$$

is generated about the hinge axis, $x$. In eq. (10), the integration is extended over the wing span, $b$, and $m$ is the structural density. $R_{A_i}(s, \eta)$ refers to the components of the wing position at the curvilinear coordinate $s$ (in the body-attached frame $A$, Fig. 1). This is computed starting from the positions and rotations of the FEs discretising the wing, $\eta$. Therefore, $S_y$ and $S_z$ are proportional to the position of the wing centre of mass along the $y$ and $z$ axis of the body frame $A$, respectively. In particular, $S_y \neq 0$ only if wing deflections are not symmetric, while $S_z$ increases as large bending deflections occur.

The aerodynamic rolling moment $M_{ax}$ in eq. (8) depends upon the control surfaces deflections, ($\beta_L$ and $\beta_R$), the wing roll rate $\dot{\Phi}$ and shape, $\eta$. Depending on the wing design and flight condition, a large wing dihedral may be produced. In this case, since rolling does not happen about an axis aligned along the free stream velocity, the local changes of angle of attack at the wing cross-sections will not be symmetric along the span, thus adding a new contribution to the roll dynamics. Consequently, a further dependency of $M_{ax}$ on the roll attitude, $\Phi$, has to be included.

The aerodynamic moment in eq. (8), $M_{ax}$, is computed for a given set of flight parameters $p^*$ — to which corresponds a certain wing shape $\eta(p^*)$. The moments are then linearised around $p^*$ as

$$M_{ax} = \; M_{ax}(p^*, \eta(p^*)) + q_\infty c b^2 \; C_{Mp_i}(p^*, \tilde{\eta}) \; \Delta p_i \tag{11}$$

where the stability and control derivatives with respect to the flight parameter $p_i$, with $i = 1, \ldots, 5$ are obtained here using finite-differences in the full aeroelastic model of Sec. II.A, but other estimates may also be used. Each derivative $C_{Mp_i}$ depends on the wing shape, $\tilde{\eta}$, associated to the perturbed term in eq. (11). For stiff airframes, zero deflections may be assumed, while static aeroelastic effects can be captured by setting $\tilde{\eta}$ to be the deformed wing shape at the flight point $p^*$, hence setting $\tilde{\eta} = \eta(p^*)$. To account for aeroelastic effects linked to the variations of the $i$-th flight parameter, $\Delta p_i$, the stability and control derivatives are evaluated at $\tilde{\eta} = \eta(p_i^* + \Delta p_i)$. Following this approach, elastified stability and control derivatives are obtained through finite differences on the full aeroelastic model.

## III. Rolling Dynamics of Very Flexible Wings

Key aspects of rolling manoeuvrability using very flexible wings are now investigated. To isolate the dynamic effects associated to the wing flexibility, computer models of hinged HALE wings have been built (Sec. III.A). This setting allows to keep pitch and yaw attitudes constant, such that the wing can be stabilised without horizontal and vertical tailplanes. Using the nonlinear aeroelastic description of Sec. II.A, their response to prescribed aileron deflections is first analysed as a function of the wing stiffness (Sec. III.B). This section, in particular, outlines how large bending and torsional deflections affect the rolling performance. In Sec. III.C a flight-dynamics model of the same system is assembled using elastified stability derivatives.

### III.A. Equilibrium of the Hinged Wing

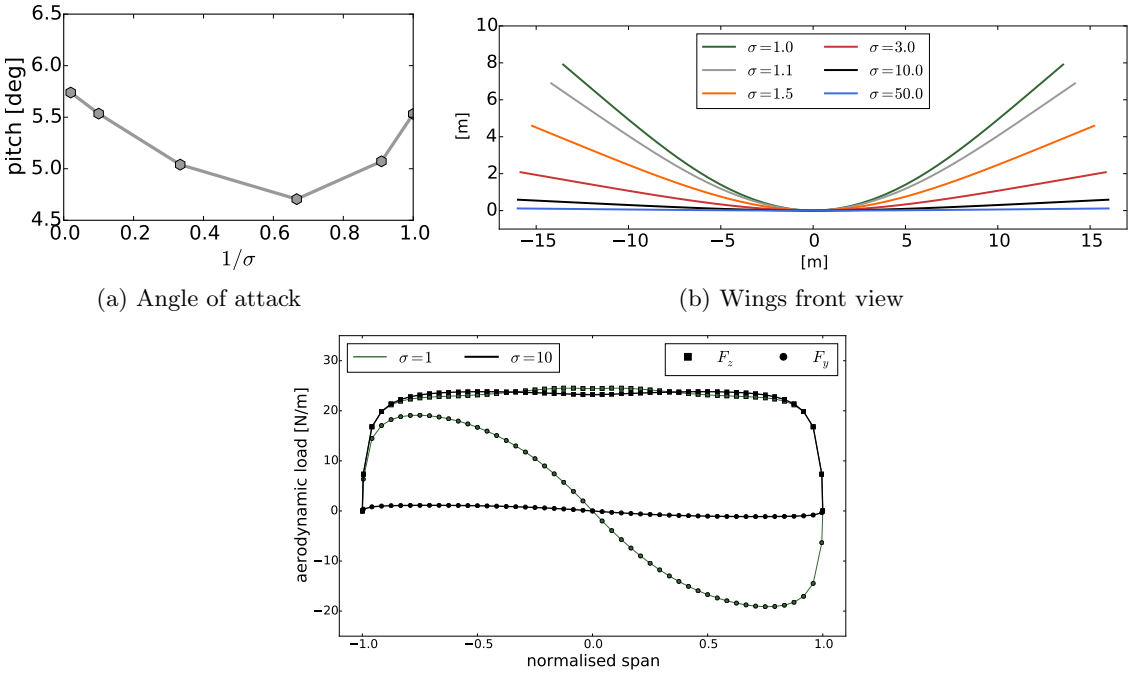
The hinged-wing model is based on the high-aspect-ratio wing configuration first introduced by Patil et al.[32] As proposed later by Murua et al.[22], and with the aim of investigating the impact of the wing flexibility on its manoeuvring performance, its stiffness is scaled by a factor, $\sigma$. The properties of the resulting model are summarised in Tab. 1. The wing is only allowed to rotate about the root chord axis hence, with reference to Fig. 2, the unit vector $\hat{c}$ lies along the $x$ axis of the body-attached frame, $A$. This implementation has been verified computing the flutter speed of the $\sigma = 1$ wing at a pitch attitude of 4 deg in both a clamped and hinged configuration. Flutter was found to occur over a velocity of $21.4\,\mathrm{m\,s^{-1}}$ with a frequency of 3.27 Hz, showing a good agreement with Patil et al,[32] who used a finite-state air-loads model.[33]

| Property | Value | |
|---|---|---|
| Wing span | 32 | m |
| Chord | 1 | m |
| Elastic axis | 0.5 | m (from leading edge) |
| Inertial axis | 0.5 | m (from leading edge) |
| Mass per unit length | 0.75 | $\mathrm{kg\,m^{-1}}$ |
| Moment of inertia | $10^{-1}$ | kg m |
| Extensional stiffness | $10^{7}$ | $\mathrm{N\,m^2}$ |
| Torsional stiffness | $\sigma \cdot 10^{4}$ | $\mathrm{N\,m^2}$ |
| Spanwise bending stiffness | $2\,\sigma \cdot 10^{4}$ | $\mathrm{N\,m^2}$ |
| Chordwise bending stiffness | $5 \cdot 10^{6}$ | $\mathrm{N\,m^2}$ |

Table 1: Hinged wing properties.

In the studies presented in this work, $\sigma$ is varied in the range $1 \div 50$ and the wing is assumed to fly at an altitude of 20 km and a speed of $30\,\mathrm{m\,s^{-1}}$. As shown in Fig. 3a, for each value of $\sigma$ the pitch attitude, measured as the angle between the wing root chord and the free stream velocity, has been adjusted so as to support a total weight of 75 kg (731.6 N). A front view of the wings in steady level fly shows that large bending deflections, comparable to the wing span, occur as the wing flexibility is increased (Fig. 3b): for $\sigma = 1$, for instance, the tip vertical deflection is above 40 % of the wing semispan, $b/2$. As better shown in Fig. 3c, these tilt the aerodynamic force sideways towards the wing symmetry plane, meaning that higher angles of attack — and thus higher aerodynamic loads — are required to provide the target lift $L = 731.6\,\mathrm{N}$. This effect is, however, counteracted by large torsional deformations, which increase the wing sections incidence at the tips. As a result, and in order for the lift to be constant, a non monotonic trend of the root chord angle of attack is observed as $\sigma$ is varied (Fig. 3a).

The instability identified above for the very flexible wings is a humped mode and at the flying speed of




(a) Angle of attack

(b) Wings front view

(c) Aerodynamic force distribution on deformed wing

Figure 3: Steady-level flight trimmed conditions for different values of the stiffness parameter $\sigma$.

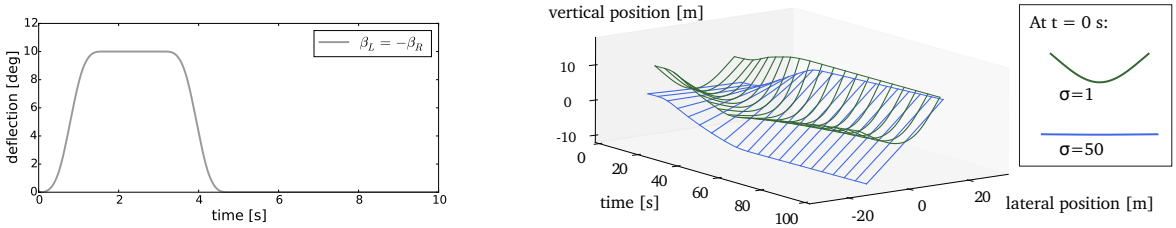
$30\,\mathrm{m\,s^{-1}}$ all wings are stable. However, as it will be shown in Sec. III.B and IV, the low frequency structural modes are only lightly damped for the most flexible wings (e.g., $\sigma \leq 1.1$). These are the vertical bending mode, which has frequency of 0.33 Hz ($\sigma = 1$) and 0.35 Hz ($\sigma = 1.1$) and the in-plane bending/torsional mode, with frequencies of 0.92 Hz and 1.10 Hz when going from a $\sigma = 1$ to a $\sigma = 1.1$ wing, respectively. The dynamics associated to these modes will be further discussed in Sec. III.B.

### III.B. Roll Dynamics under Fixed Control

The rolling performance of hinged flexible wings will be now investigated. The pitch attitude has been chosen as per Fig. 3a, such that all wings produce the same total lift, $L = 731.6\,\mathrm{N}$. Large ailerons are placed at the wing tips, extending for 25 % of the wing span and having a chordwise dimension of 25 % $c$. Rolling is induced applying an anti-symmetric aileron deflection $\beta_L = -\beta_R$ (Fig. 4a) so as to move the left (port) wing upwards — see the snapshots of the wing response in Fig. 4b. The control surfaces deflections are assumed to be positive when increasing the local lift.

For the numerical analysis, the wing structure has been discretised using 24 quadratic beam elements. The UVLM wake length has been fixed to be 20 chords and 4 chordwise panels are used for the the wing lattice.

In these studies, in fact, aeroelastic effects are associated to low values (below 0.12) of the reduced frequency $k = \frac{1}{2}\frac{\omega c}{U_\infty}$ — where $\omega \approx 7.2\,\mathrm{rad\,s^{-1}}$ is the frequency associated to the slowly damped bending/torsional modes observed for $\sigma \leq 1.1$. Also the wake roll-up has little impact on the aerodynamic loads and has been therefore neglected for limiting the computational cost associated to the optimisations in Sec. IV — the time required for each aeroelastic analysis is, in fact, reduced of roughly the 80 %. The chordwise panelling implies a single row of vortex rings modelling the ailerons: this was found sufficient to model the dynamics of the flexible wings,[26] but the increase in aerodynamic force produced by the ailerons under potential-flow assumptions is slightly underestimated.



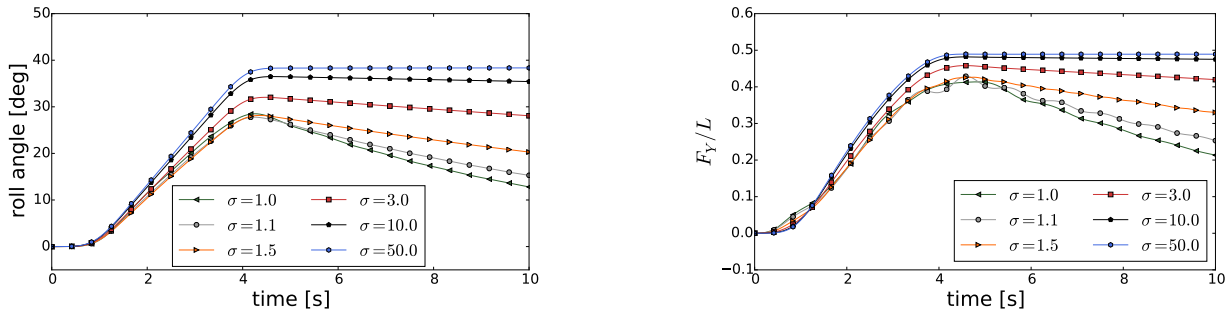

(a) Antisymmetric ailerons deflection

(b) Snapshots (2 frames per second)

Figure 4: Ailerons deflection used for the study of the rolling manoeuvre performance of flexible wings (a) and snapshots of $\sigma = 1$ and $\sigma = 50$ wings response (b).

Fig. 5 shows the roll attitude, measured at the hinge axis, and the side force, $F_Y$ — normalised with respect to the steady level flight lift, $L$ — achieved during the manoeuvre for wings of stiffness parameters ranging between $\sigma = 1$ and $\sigma = 50$. In first place, the lateral stability of a very stiff ($\sigma = 50$) hinged wing with no dihedral and sweep is briefly discussed. As observed in both Fig. 5a and Fig. 5b, this is in a neutral equilibrium position with respect to rolling: as the ailerons are retreated, the wing stabilises around a roll angle of 38.6 deg, producing a side force $F_Y = 49\,\%L$.

As the wing becomes more flexible, however, three main effects can be observed. In first place, the authority of the control surfaces is reduced: the lower $\sigma$, in fact, the smaller are the roll angle and the side force achieved during the manoeuvre (Fig. 5). Due to the large side loads associated to the wing bending, however, while the drop in roll attitude is as large as 25 % when going from $\sigma = 50$ to $\sigma = 1$, the loss of maximum lateral force is just below 13 %. In a second phase, a stabilising moment, which tends to restore the original roll attitude, arises once the ailerons are retreated. Again, this effect intensifies when deflections are larger: while the stiffer wing ($\sigma = 50$) maintains a constant side force at the end of the manoeuvre, the decay rate is as high as $23.7\,\mathrm{N\,s^{-1}}$ for the most flexible one ($\sigma = 1$). For $\sigma = 1.1$ and $\sigma = 1.0$, furthermore, the




(a) Roll attitude

(b) Lateral force

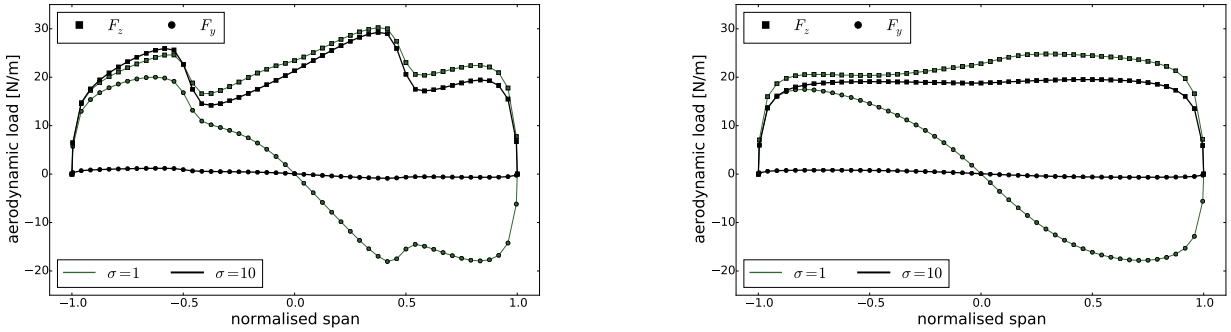
Figure 5: Roll attitude and lateral force time history for an ailerons antisymmetric deflection with different values of the stiffness parameter $\sigma$.

wing in-plane bending/torsional mode is excited, leading to slowly damped oscillations of the time history of the lateral force. In the remaining part of this section, all these effects are discussed in more detail.

The reduction in control authority is mainly due to large torsional deformations, which is essentially a linear aeroelastic effect. Their negative impact is understood by looking at wing loads during the manoeuvre. Fig. 6a compares the aerodynamic loads 3 s into the rolling manoeuvre — when the ailerons are fully deployed and the rolling rate is steady — along the span of a moderately stiff ($\sigma = 10$) and a flexible ($\sigma = 1$) wing. To allow for a fair comparison, the force components are projected on the body frame A. The sudden change in lift per unit span produced by the ailerons deflection is considerably smaller for $\sigma = 1$, thus reducing the net rolling moment with respect to the rigid wing. The effect is caused by adverse torsional deflections. These are observed in Fig. 7a, where the $y$ component of the Cartesian rotation vector at the tips of a $\sigma = 1.1$ wing is used to quantify the amount of torsion. Also the center wing load distribution acts against rolling (Fig. 6a): this effect is, however, associated to the wing roll rate.

Large bending deflections have a small impact in reducing the control authority. This is connected to the fore-shortening effect:[34] as bending increases, the wing tips get closer to the axis of rotation, thus reducing the ailerons moment arm. Asymmetric wing deflections, however, amplify this effect. During rolling, in fact, the right wing (moving downwards) stretches up, as the bending load decreases. On the other hand, the port wing (which also experiences a small reduction in loads due to the decrease in effective angle of attack associated to the rigid-body rotation) maintains a larger bending and, therefore, a stronger fore-shortening effect. The resulting asymmetry is shown in Fig. 7b for a $\sigma = 1.1$ wing. Finally, it is worth noticing that in this configuration the reduction in control authority occurring in the more flexible wings is partially stemmed by the gravity force. For low values of $\sigma$, in fact, the wing center of mass is raised above the axis of rotation,

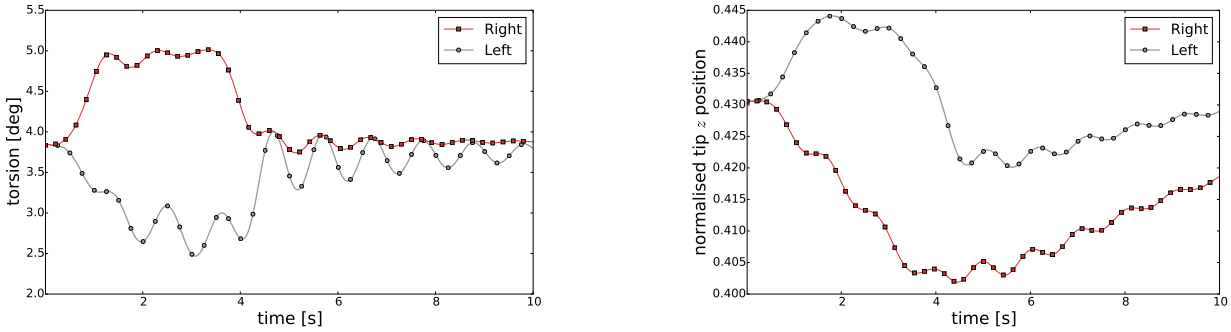
hence gravity provides a positive contribution to roll — see also eq. (9).




(a) $t = 3$ s

(b) $t = 6$ s

Figure 6: Comparison of loads distribution at different times of the rolling manoeuvre for wings having a stiffness of $\sigma = 1$ and $\sigma = 10$.




(a) Tip torsion angle (positive when the leading edge moves upwards)

(b) Tip vertical position (positive in upwards direction)

Figure 7: Tip bending deflection (normalised by the semi-wing span) and torsion during a rolling manoeuvre for a wing of stiffness parameter $\sigma = 1.1$.

The stabilising rolling moment observed in Fig. 5 once the aileron deflection is returned to zero is also connected to the bending deformations, which, effectively, give the wing a dihedral angle. As the axis of rotation is not aligned with the air stream, the cross sections of the starboard wing, moving downwards, will have a higher angle of attack than those of the left wing. This is observed in Fig. 6b, where the span-wise aerodynamic load distribution at time $t = 6$ s, i.e. when the ailerons are not longer deflected, is shown. While the stiffer wing shows a symmetric loads distribution, the flexible one has higher lift on the right side. It is worth underlining that this effect would also be observed on a rigid wing with dihedral angle, but would disappear if the wings rotate about an axis parallel to the free air stream velocity. Asymmetric deflections also increases the magnitude of the stabilising moment. As seen in Fig. 7b for $\sigma = 1.1$, as the wing rolls

back ($t > 4\,\mathrm{s}$), its right side remains more stretched. This, together with the damping effect produced by the rolling rate, guarantees a higher local angle of attack than on the left wing.

During the second phase of the manoeuvre, torsional deflections do not produce significant differences in local angle of attack between left and ring wing (see Fig. 7a, $t > 4\,\mathrm{s}$). The time histories of the tip torsion show, however, that for $\sigma = 1.1$ in-plane bending/torsional mode are excited with a frequency of oscillations of around 1.05 Hz. Vibrations are significantly stronger on the left wing (moving upward). Here, in fact, bending deflections are larger: the frequency of the torsional mode is, therefore, reduced,[32;35] and the torsion/bending coupling is facilitated. Contrarily, on the right wing, vibrations are smaller amplitude and damp faster Fig. 7a and 7b). As observed in Fig. 5b, the left wing vibrations have an impact on the manoeuvre, as they cause the lateral force to oscillate for $t > 3\,\mathrm{s}$. For $\sigma = 1.1$, the wing has bent quite significantly, hence the changes in aerodynamic force produced by the local changes of angle of attack from wing torsions directly translate into variations of the overall lateral force, $F_Y$.

Overall, the reduction in control authority observed in very flexible wings can be mainly attributed to the wing torsion, which is a linear aeroelastic effect. Geometrical nonlinearities from the wing bending may also have an important impact on the rolling dynamics. In particular, the effective dihedral associated to large bending of the very flexible wings produces asymmetric changes of the local angle of attack between left and right wing, hence, if the axis of rotation is not aligned with the flow speed, a stabilising moment is observed even in absence of side-slip. Also, as the wing bends there are larger bending/torsional couplings, which results in more complex ("instantaneous") mode shapes.

### III.C. Elastified Stability Derivatives

A simplified EFDM of the hinged flexible wings is built next by linearising the aerodynamic moment around the steady level flight equilibrium position $p^* = (\Theta^*, 0, 0, 0, 0)$, where $\Theta^*$ is prescribed as per Fig. 3a. While the accuracy of this description decreases as the importance of elastic effects grows, the EFDM model will allow for a further insight into the physics of lateral manoeuvres and to quantify geometrically nonlinear effects. To populate eq. (11), the wing stability derivatives are evaluated around $p^*$ by finite differences on the nonlinear aeroelastic model of Sec. II.A while allowing for large deflections.

Fig. 8 shows the stability derivatives measured when including (*elastified*) or not (*rigid*) the effect of elastic deformations — hence, with reference to eq. (11), when evaluating the perturbed moment assuming $\tilde{\eta} = \eta(p^*)$ and $\tilde{\eta} = \eta(p^* + \Delta p)$, respectively. Note that the stability derivatives in Fig. 8 correspond to the same lift (and different angles of attack, as shown in Fig. 3a). As expected, the most important terms

are the control derivative $C_{M_\beta}$ and the damping term $C_{M_{\dot{\Phi}}}$ associated to the roll rate of change $\dot{\Phi}$. The derivative associated to the roll attitude $C_{M_\Phi}$ was, instead, found to be relatively small, yet non negligible, for very flexible designs. This term introduces the restoring moment for wings of low $\sigma$ value. The damping coefficient associated to the roll rate, $C_{M_{\dot{\Phi}}}$, has an almost 50 % reduction when going from a $\sigma = 50$ to a $\sigma = 1$ wing, but no major difference is observed when elastifing it, meaning that this contribution is mainly connected to the large bending deflections of the wing in steady level flight. While $C_{M_\Phi}$ and $C_{M_{\dot{\Phi}}}$ do not show significant variations when allowing for aeroelastic corrections, however, the control authority, $C_{M_\beta}$, is drastically reduced as the wing flexibility increases. As discussed in Sec. III.B this important effect is mainly driven by the adverse twist produced by the ailerons (Fig. 7a). The small drop of the rigid $C_{M_\beta}$ (around 5 % when passing from a $\sigma = 50$ to a $\sigma = 1$ wing), results, instead, from the fore-shortening effect. Although the rolling moment generated by gravity can be computed exactly via eq. (9), the term

$$C_{M_g} = \frac{1}{q_\infty c b^2} \frac{\partial M_{gx}}{\partial \Phi} \tag{12}$$

has also been included in Fig. 8 to show that, despite the wing roll axis not passing through its center of mass, gravity has little importance in these cases. Also, the elastified $C_{M_g}$ trend overlaps with the rigid one, proving that changes of $I_{xx}$, $S_y$ and $S_z$ in eq. (8) and (9) are here almost negligible.

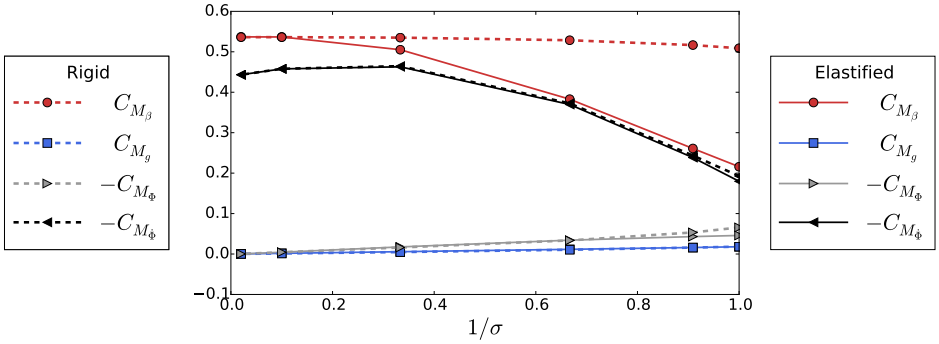



Figure 8: Rigid and elastified stability derivatives for wings of different flexibility, $\sigma$, around a level flight equilibrium point.

Substituting the elastified stability derivatives of Fig. 8 into eq. (8) and (11) leads to the following equation for the hinged wing roll dynamics:

$$I_{xx}\ddot{\Phi} - q_\infty c b^2 \left( C_{M_{\dot{\Phi}}} \dot{\Phi} + C_{M_\Phi} \Phi \right) = M_{gx}(\Phi) + q_\infty c b^2 C_{M_\beta} \beta(t) \tag{13}$$

where $M_{gx}$ is computed according to eq. (9). In order to compare the predictions of the EFDM model against the results obtained through a full aeroelastic analysis (Sec. III.B), however, the lateral force, $F_Y$, is also required. This is obtained as a post-processing step once eq. (13) is solved with respect to $\Phi$. To this aim, the vertical force in the body frame $A$ is assumed to be proportional to the wing root angle of attack, $\alpha$. At each roll attitude, $\alpha$ is given by

$$\alpha(\Phi) = \arctan\left(\frac{\hat{u}\cdot\hat{n}(\Phi)}{\hat{u}\cdot\hat{c}}\right) \tag{14}$$

where $\hat{c}$ and $\hat{n}$ are the unit vectors parallel and normal to the wing root chord (Fig. 2) and $\hat{u}$ is aligned with the free-stream velocity. All quantities are projected in $G$ coordinates, hence only $\hat{n}$ depends on the roll angle as the wing rolls about $\hat{c}$. Scaling and rotating the steady level flight lift, $L$, allows to express the lateral force in the inertial frame $G$ as

$$F_Y = \sin\Phi\frac{\alpha(\Phi)}{\alpha(0)}L \tag{15}$$

where $\alpha(0) = \Theta^*$ is the wing root angle of attack at the beginning of the manoeuvre (Fig. 3a).

In Fig. 9 the lateral force, $F_Y$, predicted by eq. (15) as a function of the roll attitude, is compared against the one resulting from the rolling manoeuvres presented in Fig. 5 and computed via a full aeroelastic analysis. The differences between a very flexible ($\sigma = 1$) and a very stiff ($\sigma = 50$) wing are very small, although eq. (15) does not capture the small hysteresis observed for $\sigma = 1$, which are mostly due to changes in wing inertia due to the large displacements. In this can, in fact, due to the large bending, the extra aerodynamic load produced by a deflection of the ailerons contributes to the lateral force even when the wing is close to its steady level flight configuration ($\Phi \to 0$, Fig. 3b). This effect is also observed in the lateral force time histories in Fig. 5b around $t = 1\,\mathrm{s}$, and vanishes for large $\sigma$ as the wing dihedral diminishes.

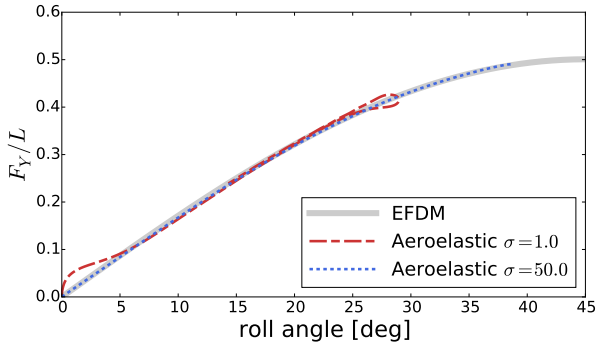
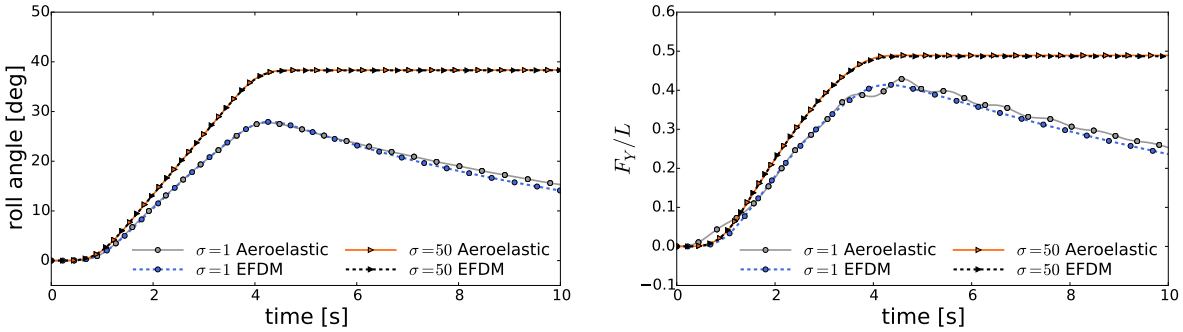



Figure 9: Total lateral force, expressed as a function of roll attitude through the analytical relation (15) and through a full aeroelastic analysis, for a very flexible ($\sigma = 1$) and a stiff ($\sigma = 50$) wing.

The wing response to the antisymmetric ailerons deflection in Fig. 4a can now be approximated using the elastified flight-dynamics equations (13) and (15). The comparison against the nonlinear aeroelastic solution of Sec. III.B is shown in Fig. 10 for $\sigma = 1$ and $\sigma = 50$. As expected, when geometrically-nonlinear effects are negligible ($\sigma = 50$), both models are in excellent agreement. As these become important, however, some differences can be observed, mostly during the second phase of the manoeuvre ($t > 4\,\mathrm{s}$). Fig. 11 shows the contribution to the total moment for $\sigma = 1$ from each term in eq. (13). During the initial phase of the manoeuvre (ailerons fully deflected, $t < 4\,\mathrm{s}$), the most significant ones are the ailerons input and the roll rate damping. The good match against the nonlinear aeroelastic response shows that the impact of the adverse torsional deformations — produced by the deflection of the control surfaces (Fig. 7a) — is well capture through the elastification of the $C_{M_\beta}$ derivative. Importantly, this also proves that this effect remains predominantly linear despite the large changes in wing shape occurring during the manoeuvre (Fig. 7b). Also the roll rate damping is well estimated. As the aeroelastic correction only accounts for instantaneous geometry changes, it is clear that the nominal manoeuvre for this configuration is slow enough for aeroelastic effects to remain quasi-stationary.




(a) Roll attitude

(b) Side force normalised with respect to the total lift at $t = 0\,\mathrm{s}$ (731.6 N)

Figure 10: Wing response to an antisymmetric aileron deflection from elastified flight-dynamics model and full aeroelastic analysis.

For $t > 4\,\mathrm{s}$ the restoring moment associated to the roll attitude becomes predominant, while the impact of gravity is rather limited (Fig. 11). In the EFDM description, however, this is over-predicted, leading to a growing error in the roll response (Fig. 10a). The elastification of the $C_{M_\Phi}$ derivative, therefore, does not fully capture the geometrical nonlinearities associated to this phase of the manoeuvre, namely the asymmetries in wing bending deflections and the resulting changes of local angle of attack (Sec. III.B). Regarding this, it is worth recalling that the aeroelastic correction has little effect on $C_{M_\Phi}$ (Fig. 8), as it only accounts for

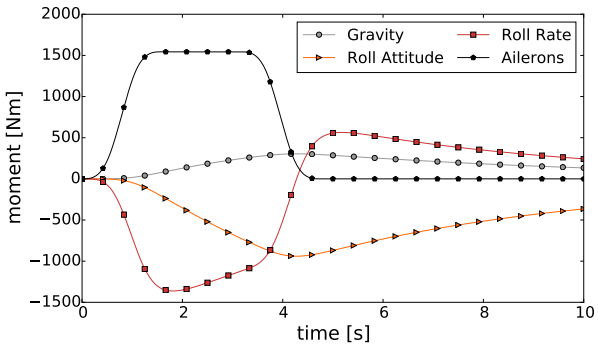



Figure 11: Decomposition into the terms appearing in eq. (13) of the total rolling moment for $\sigma = 1$ under the aileron deflection defined in Fig. 4a.

the static effects. The small inconsistency between the EFDM and the full aeroelastic prediction, therefore, indicates that the coupling between rigid and flexible dynamics — only captured by the latter model — becomes more important in this phase.

Overall, the EFDM is seen to give a good approximation for the rolling dynamics even for very flexible wings. The main drawback of this simplified description is clearly that no structural dynamics is captured; for instance, the oscillations of lateral force linked to the wing torsional/bending dynamics are lost (Fig. 10b). When seeking optimal manoeuvres on very flexible wings, this will imply severe constraints on actuation bandwidth that may limit performance, as will be seen in the next section.

## IV. Optimal Control of Flexible Wings

Results in Sec. III.B have shown that, even for a rather simple aileron commands, the response of very flexible wings can be quite involved. The task of scheduling aileron deflections becomes, therefore, more elaborate, especially when the aim is to identify manoeuvres for best performance under a given metric. In this section they will be obtained from the solution of an optimal control problem. In Sec. IV.A, time histories of aileron commands obtained through this approach will be compared against those identified using the simplified elastified flight-dynamics description. This comparison will assess the single-shooting based framework and assess the relative importance of geometrically-nonlinear effects and structural dynamics when designing manoeuvres with very flexible wings.

When using the single-shooting approach, the best-performing rolling manoeuvres are obtained as a solution to the optimal control problem (3). Defining a rolling manoeuvre for a flying wing typically requires a trade-off between competing performance objectives, hence leading to an inherently multi-objective problem.

In order to recast this into a problem of the form (3), the cost function, $I$, is scalarised and expressed as a weighted sum of multiple objectives, $I_j$,

$$I = \sum_j w_j I_j \tag{16}$$

In all the study proposed, the objective to roll the wing until a target lateral force $F_T$ — equal to the 40 % of the steady level flight lift, $L$ — is produced. Two variations of this manoeuvre are considered. Firstly, the focus is in rolling the wing as fast as possible while minimising wing vibrations and control effort. This formulation, which requires dividing the manoeuvre into segments, is used in for assessing the single-shooting framework in Sec. IV.A and discussed in more detail in Sec. IV.B. A second study will instead investigate strategies to compromise large gains in lateral force with a moderate lift loss (Sec. IV.C). In both cases, the deriving optimisation problem is inherently multi-objective, as a trade-off between conflicting requirements is necessary (namely short transient vs. low vibrations and large lateral force vs. low lift loss). This aspect is expressed in the optimisation problem by defining the cost function $I$ as a weighted sum of multiple objectives, eq. (16). The impact of the wing flexibility on the optimal actuation is also investigated by defining the manoeuvre for wings of different stiffness parameters $\sigma$.

All wings are again assumed to fly at a speed of $30\,\mathrm{m\,s^{-1}}$ and their pitch attitude is adjusted so as to produce the same lift, $L$, in steady level flight (Fig. 3a). In all the optimisation studies the ailerons are initially set to zero angle and, unless otherwise stated, this has been parametrised using 2 control points per second, thus achieving a maximum nominal excitation frequency $f_{max} = 1\,\mathrm{Hz}$. For the most flexible wings ($\sigma \leq 1.1$) this resolution is enough to capture the first bending (around 0.3 Hz) and in-plane bending plus torsional mode (around 1 Hz). Finally, the maximum travel limit and rate of deflection in eq. (4) are set to be, respectively, $\beta_{max} = 10\,\mathrm{deg}$ and $\dot{\beta}_{max} = 15\,\mathrm{deg\,s^{-1}}$.

### IV.A. Assessment of the Optimal Control Approach

In this first study, aileron commands are constrained to be antisymmetric ($\beta_L = -\beta_R$) and the optimal control description is achieved decomposing the rolling manoeuvre into two segments. During the initial, transient, stage ($t < T_s$), the control is asked to move the system from one equilibrium point (steady level flight) to another (wing at constant roll attitude): the aim is to achieve this as quickly as possible, hence no penalty is imposed on the amount of actuation required. In the second segment ($t \geq T_s$), the main objective is to stabilise the wing maintaining the lateral force constant. During this phase a penalty is associated to the control surfaces rate of deflection, $\dot{\beta}$. Importantly, this aims to guarantee not only a cheap actuation

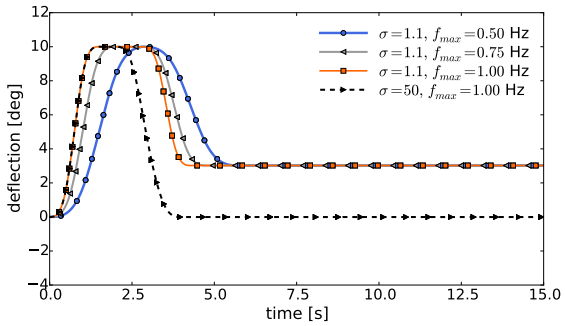
strategy, but also that the control leads the system towards a steady state (wing rolled with $\dot{\beta} = 0$). Using a quadratic norm to measure the gap between the instantaneous lateral aerodynamic force, $F_Y$, and the target force, $F_T$, the cost function, $I$, is therefore defined as:

$$I = \int_0^{T_s} w_T E(t)^2 dt + \int_{T_s}^{T} \left( w_S E(t)^2 + w_p \beta(\dot{t})^2 \right) dt \quad , \quad E(t) = F_Y(t) - F_T \tag{17}$$

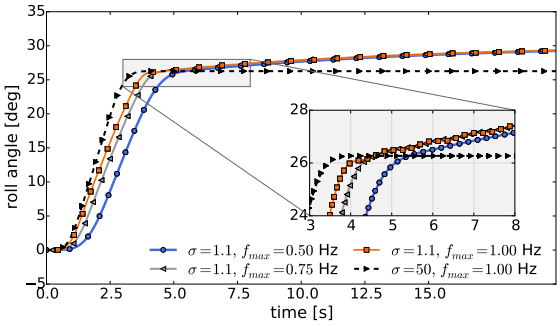
The weights in eq. (17) depend on the type of control being sought, namely how fast the response should be, how important it is to reduce vibrations during the second stage and which level of actuation can be accepted. These aspects will be discussed in Sec. IV.B. For this initial study, these are set to be $w_T = 10^{-4}\,\mathrm{N^{-2}s^{-1}}$, $w_S = 10^3 w_T$, and $w_P = 5 \times 10^{-2}\,\mathrm{deg^{-2}s}$, which were chosen after a preliminary investigation to ensure that the integral terms in eq. (17) have comparable magnitude. In particular, a relatively large weight is associated to the lateral force gap, $E$, to reduce the oscillations of this force durign the second segment of the manoeuvre. The manoeuvre is simulated for a total time $T = 15\,\mathrm{s}$. The time allowed for the transient stage, $T_s$, could be potentially defined as a result of the optimisation itself. However, this was not necessary here, as $T_s$ could be estimated from the wings responses to a prescribed control input in Sec. III.B. In particular, this was fixed to be $T_s = 5\,\mathrm{s}$ and $T_s = 4\,\mathrm{s}$ for $\sigma = 1.1$ and a $\sigma = 50$, hence being inversely proportional to the wings control surfaces authority.

A reference input can be easily derived by inspection using the simplified flight-dynamics description introduced in Sec. II.C and III.C. At the beginning of the manoeuvre, ailerons are deflected at their maximum rate and to their maximum amplitude (no penalty is enforced on the actuation), so as to roll the wing as fast as possible. The roll attitude required to produce the target lateral force, $F_T$, can be obtained through eq. (15): once this is known, the time for which the ailerons are fully deflected can be tuned. Finally, solving eq. (8) at a steady state provides the aileron inputs required to stabilise the wing roll — note that these are kept constant to minimise the penalty term in eq. (17). The time histories provided by this approach for $\sigma = 1.1$ and $\sigma = 50$ are shown in Fig. 12a. Note that the $\sigma = 1.1$ control input has been derived also for maximum nominal actuation frequencies, $f_{max}$, below 1 Hz. This parameter, in fact, determines the maximum rates $\dot{\beta}$ and $\ddot{\beta}$ on the controls (Sec. II.B) and, thus, allows to regulate how strongly the wing structural dynamics is excited.

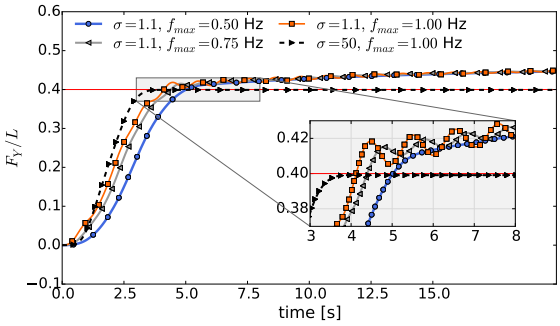
The nonlinear aeroelastic responses to the input in Fig. 12a is presented in Fig. 12b and 12c in terms of wing roll attitude and lateral force produced. These results show that, overall, the key features of the wings dynamics are always captured. The ailerons have more authority on the rigid wing, hence less actuation




(a) Ailerons deflection, $\beta_L = -\beta_R$




(b) Roll attitude



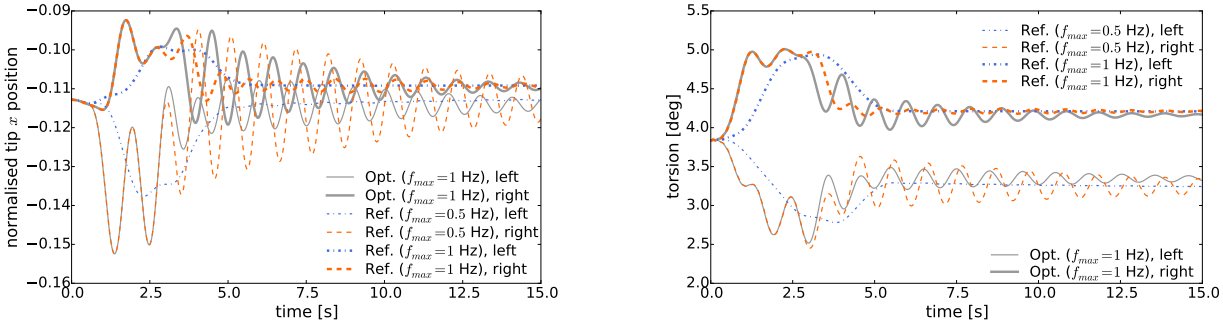

(c) Side force normalised with respect to the total lift at $t = 0\,\mathrm{s}$

Figure 12: Reference anti-symmetric actuations and aeroelastic response for wings different stiffness. The control inputs have been derived for different maximum excitation frequency, $f_{max}$, based on the EFDM description.

time is required. For $\sigma = 1.1$ the full deflection is required for a longer time and a nonzero angle is necessary at the steady state to cancel the stabilising rolling moment produced by the wing dihedral (Sec. III.B). The control input generated for $\sigma = 50$ is appropriate to reach and maintain the target lateral force $F_T$, as the EFDM description approximates well the dynamics of stiff wings. Despite the aeroelastic corrections, on the other hand, on a very flexible wing ($\sigma = 1.1$) the ailerons do not stabilise the wing around the correct roll attitude (Fig. 12b) and the lateral force is 12 % larger then required at the steady state (Fig. 12c). This reflects the findings of Sec. III.C, which showed how the EFDM model loses fidelity in the second part of the manoeuvres, when the geometrical nonlinearities linked to the asymmetries between left and right wing deflections become relevant.

Importantly, when the nominal excitation frequency is above 0.5 Hz, the lateral force $F_Y$ also has a slowly damped oscillatory behaviour, which reflects the presence of wing vibrations. As observed in Fig. 13, where the time histories of the wing tips horizontal position and torsional angle are shown, these are caused

by the in-plane bending/torsional mode becoming excited. As the EFDM includes no information on the wing vibrations and the actual frequencies vary as the wing bends, rate limits should be introduced in the definition of maneouvres with this simplified descriptions. This requires bounding both $\dot{\beta}$ and $\ddot{\beta}$ to reduce the frequency content of the control input, as shown in Fig. 12a.




(a) Tip horizontal position

(b) Tip torsion

Figure 13: Details of the $\sigma = 1.1$ wing full aeroelastic response to the ailerons input in Fig. 14.

Finally, the reference actuations provided by the EFDM description are compared to those obtained through eq. (17) in Fig. 14. The corresponding nonlinear aeroelastic responses are included in Fig. 15. For the very stiff wing ($\sigma = 50$), the aileron input obtained via single shooting correlates very well with the reference case and, therefore, the aeroelastic responses are also in excellent agreement. The only difference arises at $t \approx 3.5\,\mathrm{s}$ (see Fig. 14), when the single-shooting solution changes sign. While this control diminishes the time required for the wing to settle around its steady-state roll attitude, the reduction of the cost function in eq. (17) is minimal (below 0.1 %) and, in fact, no relevant impact on the lateral dynamics is observed (see Fig. 15). As expected, "elastification" of the stability derivatives is an adequate, and computationally cheap, approximation for the dynamics of stiff wings.

To avoid structural vibrations, the maximum actuation frequency of the $\sigma = 1.1$ reference input needed to be reduced from 1 Hz to 0.5 Hz (refer to both Fig. 12 and Fig. 13), thus cutting the maximum $\dot{\beta}$ and $\ddot{\beta}$ rates of 50 % and 75 % respectively. This, however, was not required for the control input derived via a full aeroelastic solution, which, therefore, reaches the target lateral force, $F_T$, considerably faster — the time required to produce $95\,\%F_T$ is, for instance, reduced of 16.4 %. Lateral force and roll attitude are also stabilised with great accuracy (Fig. 15): in this case, in fact, the wing structural dynamics is well captured and during the optimisation the aileron input frequency content can be adjusted accordingly (Fig. 14). As a result, the bending and torsional oscillations arising on the left (moving upward) wing are reduced without having to impose rate limits (Fig. 13). Interestingly, as the ailerons movement is constrained to be anti-

symmetric, a small level of vibration is generated on the right wing. This, however, can be further damped allowing the control surfaces to move independently, as done in Sec. IV.C.

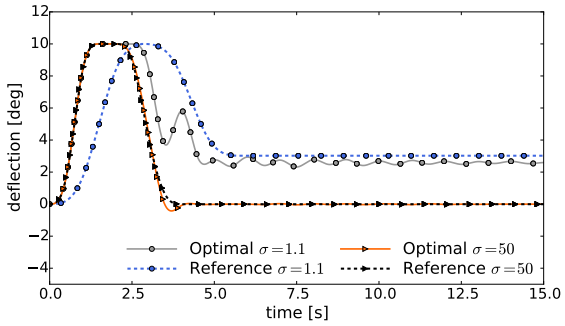
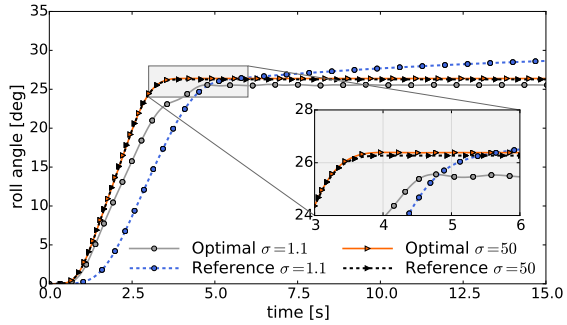
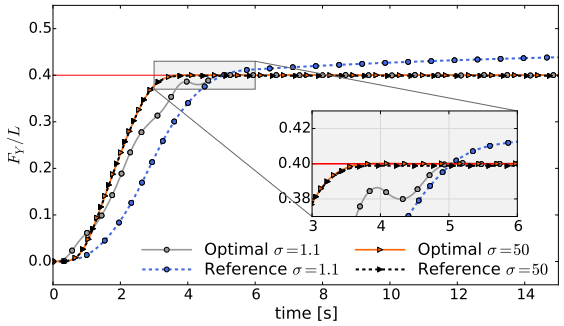



Figure 14: Optimal anti-symmetric actuations $\beta_L = -\beta_R$ for wings of different stiffness obtained via single-shooting (using a full aeroelastic model) against the reference cases (based on the EFDM description).



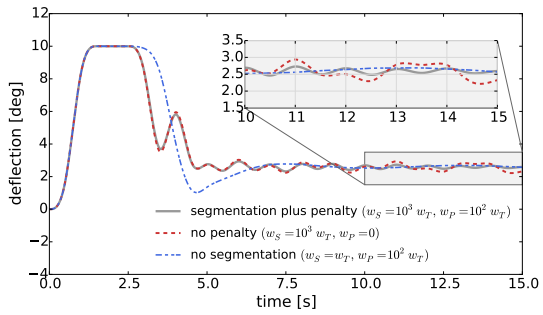

(a) Roll attitude



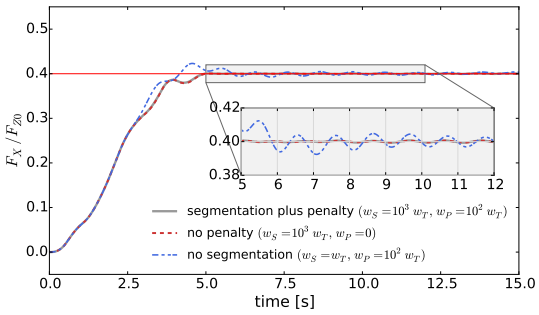

(b) Side force normalised with respect to the total lift at $t = 0\,\mathrm{s}$

Figure 15: Wings response, computed through a full aeroelastic analysis, to the ailerons input in Fig. 14.

Overall, optimisation on the full aeroelastic description managed to overcome the limitations of the elastified flight-dynamics model. In first place, this is higher fidelity and accounts for geometrical changes occurring during the manoeuvre: while negligible for stiff wings — where, in fact, the EFDM approximation is excellent — these have been shown to be relevant for very flexible ones. Most importantly, building the open-loop control upon a full aeroelastic description allows to consider more aggressive — and better performing —actuation input. The EFDM model, in fact, can not account for the wing elastic dynamics and how this interacts with the rigid dynamics. As a result, for $\sigma = 1.1$ the ailerons input based on this description can lead to wing vibrations, strong enough to be observed in the $F_Y$ time history. When using a purely flight-dynamics description, therefore, the actuation frequency must be bounded in the frequency domain, so as not to excite lowly damped structural modes. This limitation becomes even more strict as




(a) Aileron deflections, $\beta_L = -\beta_R$




(b) Lateral force

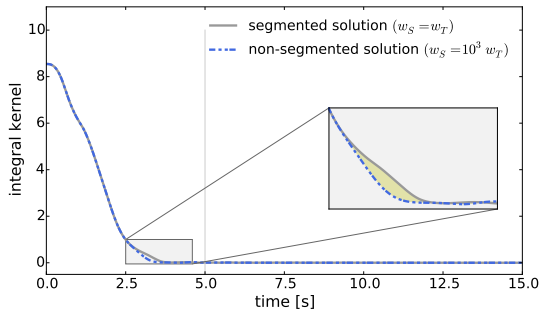
Figure 16: Impact of segmentation in defining the optimal actuation on a very flexible wing.

the original wing shape is altered during manoeuvring and the natural frequencies of its structural modes change. The nonlinear aeroelastic analysis, instead, can explore scenarios in which structural vibrations may occur during manoeuvring, which is a realistic hypothesis for novel, lighter and lighter, airframes.

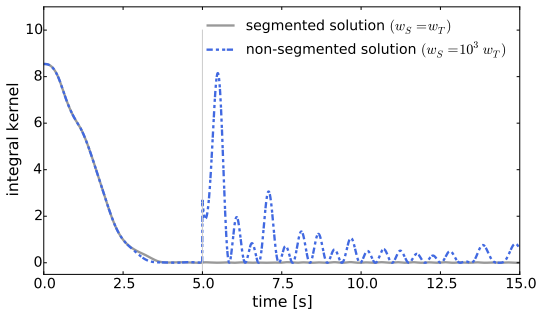
### IV.B. Trade-off between Fast and Smooth Wing Response

In the previous section, a *segmented* formulation has been chosen for defining the cost associated to the rolling manoeuvre, eq. (17). During the second segment, the actuation is penalised ($w_P \neq 0$) and a larger weight, $w_S = 10^3 w_T$, is associated to the lateral force error $E = F_Y - F_T$ (segmentation). This cost function ultimately reflects a trade-off between having a fast response during the first stage of the manoeuvre and an accurate lateral force tracking in the second phase. This concept is illustrated for a very flexible wing ($\sigma = 1.1$). To this aim, the optimal time histories of aileron commands have been computed when, respectively, removing the actuation penalty — i.e. setting $w_P = 0$ while keeping $w_S = 10^3 w_T$ in eq. (17) — and dropping the segmentation hypothesis — i.e. assuming $w_S = w_T$ as $w_P \neq 0$. The resulting aileron input, and the associated wing responses, are compared to those obtained employing a segmented formulation with penalty in Fig. 16.

When equal weights are applied to the transient and final stages of the manoeuvre (no segmentation, $w_S = w_T$), the most aggressive control is generated. The ailerons, in fact, are deflected to their maximum for a longer period (Fig. 16a), leading to a faster increase of the lateral force, $F_Y$ (Fig. 16b). On the other hand, however, $F_Y$ overshoots and small amplitude oscillations around the target lateral force value, $F_T$, appear in the second segment of the manoeuvre as the wing vibrates (Fig. 16b). This behaviour occurs as the optimiser minimises the only relevant contribution to the cost associated to the manoeuvre, namely the error accumulated during the transient stage ($t < T_S = 5\,\mathrm{s}$). This reduction can be observed in Fig. 17a,




(a) Kernel computed assuming $w_S = w_T$ for optimal manoeuvres derived with ($w_S = 10^3 w_T$) and without ($w_S = w_T$) cost function segmentation.




(b) Kernel computed assuming $w_S = 10^3 w_T$ for optimal manoeuvres derived with ($w_S = 10^3 w_T$) and without ($w_S = w_T$) cost function segmentation.

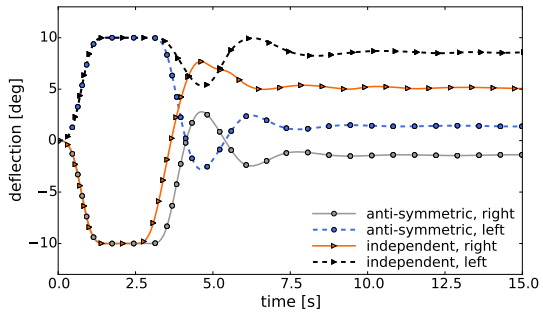
Figure 17: Integral kernel of eq. (17) for optimal manoeuvres obtained with and without segmentation of the cost function. The kernel is evaluated for different values of the weight $w_S$, associated to the lateral force error during the second stage of the manoeuvre.

where the kernel of the cost integral in eq. (17)

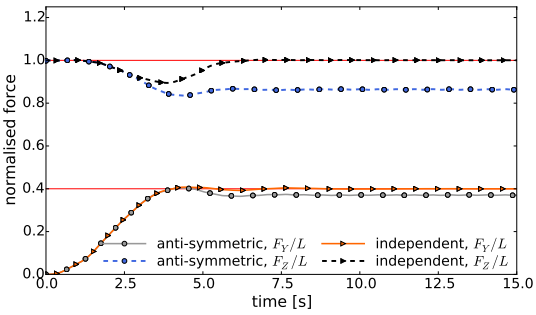
$$k(t) = \begin{cases} w_T \left(F_Y(t) - F_T\right)^2 & t \leq T_s \\ w_T \left(F_Y(t) - F_T\right)^2 + w_P \dot{\beta(t)}^2 & t > T_s \end{cases} \tag{18}$$

is compared against the one associated to aileron input and wing response obtained through a segmented formulation. From the same figure it can be observed that, as a low weight is associated to the error $E = F_Y - F_T$, the small amplitude oscillations of $F_Y$ for $t > 5\,\mathrm{s}$ do not produce relevant increases to the integral kernel. At the optimiser level, therefore, no advantage is seen in damping the wing vibrations. As shown in Fig. 17b, on the other hand, a non-negligible error would be produced if a segmented formulation was used, hence explaining why a segmented formulation allows to maintain the lateral force, $F_T$.

So far it has been shown that, if the weight associated to the lateral force error accumulated during the second phase of the manoeuvre ($w_S$) is large enough, wing vibrations are controlled whether the actuation is penalised or not (Fig. 16b). However, the control surfaces time histories in Fig. 16a show that only when a penalty is also enforced on the actuation the system also tends to a steady state. In this case, in fact, not only $F_Y$ but also the aileron commands reach a constant value, settling around $\beta_L = -\beta_R = 2.6\,\mathrm{deg}$. Otherwise, undamped, small amplitude, oscillations appear. This, in particular, reveals that multiple solutions exist and that the penalty term enforced on the rate of actuation allows to select, amongst them, the one compatible with a steady state.




(a) Aileron deflections




(b) Lateral and vertical forces

Figure 18: Optimal ailerons input, and wing response, associated to the lift-constrained rolling manoeuvre of a $\sigma = 1.5$ wing when setting an anti-symmetric and independent movement of its control surfaces.

### IV.C. Unconventional Manoeuvres - Combining Lateral and Vertical Dynamics

The versatility of the optimal control approach allows us to investigate also unconventional actuation strategies and gain a better understanding of the limit performance of very flexible wings. In order to illustrate this, the rolling manoeuvre is reformulated for exploring the trade-off between achieving a target lateral force and limiting the lift loss associated to rolling. This could also be obtained by increasing the flying speed or the vehicle pitch attitude, but here ailerons will be exploited to produce additional lift. This leads to the following cost function

$$I = \int_0^T \left[ w_Y \left( F_Y(t) - F_T \right)^2 + w_Z \left( F_Z(t) - L \right)^2 \right] dt \tag{19}$$

where the objective is to minimise measure the gap in lateral and vertical force. Their relative importance is weighted through $w_Y = 10^{-4}\,\mathrm{N^{-2}s^{-1}}$ and $w_Z = 0.5 w_R$; no other term (e.g. actuation penalty and/or segmentation) has been added in order to keep the problem simple. The manoeuvre is initially defined and analysed for a wing of intermediate stiffness ($\sigma = 1.5$): in a first case, anti-symmetric aileron deflections are enforced, while in second one these are allowed to move independently. The optimal ailerons input obtained, and the corresponding time histories of lateral and vertical aerodynamic forces, are shown in Fig. 18.

During the initial part of the manoeuvre ($t < 2.5\,\mathrm{s}$), the cost in eq. (19) is dominated by the lateral force error, $F_Y - F_T$: even when ailerons are allowed to move independently, therefore, these are deflected in opposite directions and to their maximum amplitude, so as to produce the largest achievable rolling moment (Fig. 18a). As a steady state is approached, however, two considerably different configurations are reached. When control surfaces deflections are enforced to be anti-symmetric, their amplitude at the end

of the manoeuvre is uniquely determined: in fact, for a given roll attitude, there exist only one amplitude $\beta_L = -\beta_R$ capable of stabilising the wing — i.e. to counteract the rolling moment associated to the wing dihedral (Sec. III.B). As a result, the trade-off in eq. (19) is achieved by reducing the roll angle — and the lateral force, $F_Y$ — so as to increase the lift force (Fig. 18b): at the steady state these are $F_Y = 93\,\%L$ and $F_Z = 88\,\%L$. It is worth noticing that these values depend on the relative weight between $w_Y$ and $w_Z$.

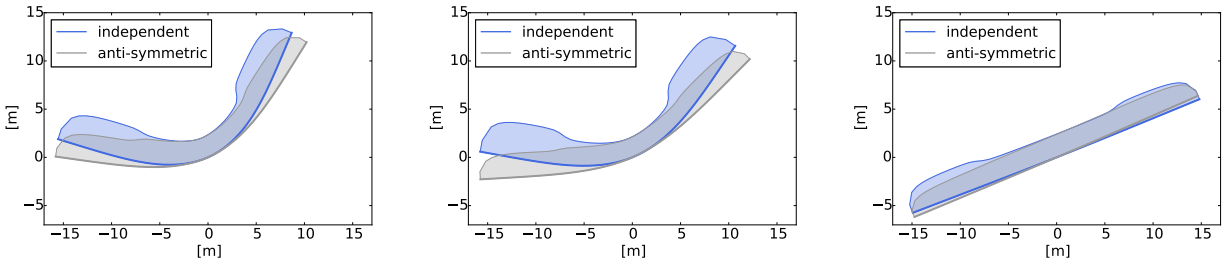
If the control surfaces can move independently, instead, once the wing has been rolled (and, hence, the error term associated to the lateral force minimised), both ailerons are deflected downwards, so as to increase the local aerodynamic force. As a result, a larger wing dihedral is produced. This is shown in Fig. 19b by comparing the wing deformed reference line at the end of the manoeuvre — and the corresponding aerodynamic load distribution — to the one obtained with anti-symmetric aileron deflections. In this configuration, the lateral loads associated to the wing curvature can be exploited efficiently. The left wing, which is almost aligned with the horizontal direction, provides a major contribution to the total vertical force, while the right wing — whose tip has an angle of 56 deg with respect to the horizontal line — mainly generates lateral force. As a result, from $t \approx 6\,\mathrm{s}$ the full target lateral force $F_T$ is achieved without any lift loss.

It is worth remarking that the control surfaces not only increase the wing curvature, but they also provide an important contribution to the total aerodynamic force (Fig. 19b) and maintain the wing attitude. At the end of the manoeuvre, in fact, left and right ailerons have a different deflection (Fig. 18a), so as to counteract the stabilising moment associated to the wing dihedral. While the key feature of this manoeuvre is that the wing shape is morphed, the deflections time histories are also optimised: from Fig. 18a, for instance, it can be observed that the right aileron is deflected to the maximum amplitude for a shorter time then the left one, as a large change of incidence is required to reach its final position (at an angle of approximately 5 deg).

The impact of the wing stiffness on the lift-constrained manoeuvre is finally investigated. To this aim, the performance, measured in terms of steady state lateral and vertical force, of wings of different stiffness is compared in Tab. 2 for cases where the control surfaces can moved independently or anti-symmetrically. When enforcing anti-symmetric commands, performance directly improves with the wing flexibility. Here,

| Wing stiffness | Anti-symmetric | | Independent | |
|---|---|---|---|---|
| | $F_Y/F_T$ | $F_Z/L$ | $F_Y/F_T$ | $F_Z/L$ |
| $\sigma = 1.1$ | 0.93 | 0.88 | 0.93 | 0.90 |
| $\sigma = 1.5$ | 0.93 | 0.86 | 1.00 | 1.00 |
| $\sigma = 50$ | 0.90 | 0.85 | 1.00 | 1.00 |

Table 2: Steady state performance of wings of different stiffness $\sigma$ when allowing, or not, the control surfaces to move independently. Note that $F_T = 0.4L$.




(a) $\sigma = 1.1$ (b) $\sigma = 1.5$ (c) $\sigma = 50$

Figure 19: Front view of the aerodynamic loads acting on a wings of different stiffness parameter, $\sigma$, at the end of a rolling manoeuvre performed using both anti-symmetric and independent aileron commands.

a flexible wing ($\sigma = 1.1$) shows increases above 3 % of both lateral and vertical force with respect to the stiff wing ($\sigma = 50$). Flexible wings can, in fact, exploit the aerodynamic side loads associated to the large curvature (as shown in Fig. 3c) to limit the lift losses associated to roll while still producing high lateral forces.

For $\sigma = 1.5$, it has already been shown that the target lateral and vertical forces can be fully maintained with independent aileron commands. In this case, in fact, the control can adjust not only the steady state roll attitude, but also the wing shape and the aileron deflections. A similar result is obtained also when the wing is stiffer ($\sigma = 50$): as shown by the loads distribution in Fig. 19c, however, in this case the wing has no dihedral, hence only the (large) ailerons are used to compensate for the lift losses. Results in Tab. 2 for $\sigma = 1.1$ underline, however, the existence of a critical value of stiffness below which, regardless of the actuation strategy adopted (independent vs. anti-symmetric deflections) the wing rolling performance is bounded and both lateral and vertical forces are largely below the respective target values.

This phenomenon is associated to the fact that the control surfaces can not be deflected enough to compensate the deficit in vertical and lateral force without producing an excessively large dihedral. To assess this, the roll attitude and steady-state forces produced for $\sigma = 1.1$ (tip displacement in steady flight over 40%) have been sampled in Fig. 20a for different amplitudes of the deflections on left and right ailerons , $\beta_L$ and $\beta_R$. In order to provide a term of comparison, the same has been done in Fig. 20b for $\sigma = 1.5$ (level-flight tip displacement just below 30%). In both figures, points $A$ corresponds to aileron deflections obtained at the steady state by solving the optimal control problem in eq. (19). It is worth noticing that the space has been conveniently sampled in terms of $\beta_L + \beta_R$ and $\beta_L - \beta_R$: the first term, in fact, is proportional the amount of lift produced by the ailerons, while the second is linked to the lateral dynamics. This can be more clearly observed in Fig. 21, where the $\sigma = 1.1$ wing deformed configuration, and the associated aerodynamic loads, corresponding to the points $A$, $B$, $C$ and $D$ of Fig. 20a have been compared to each

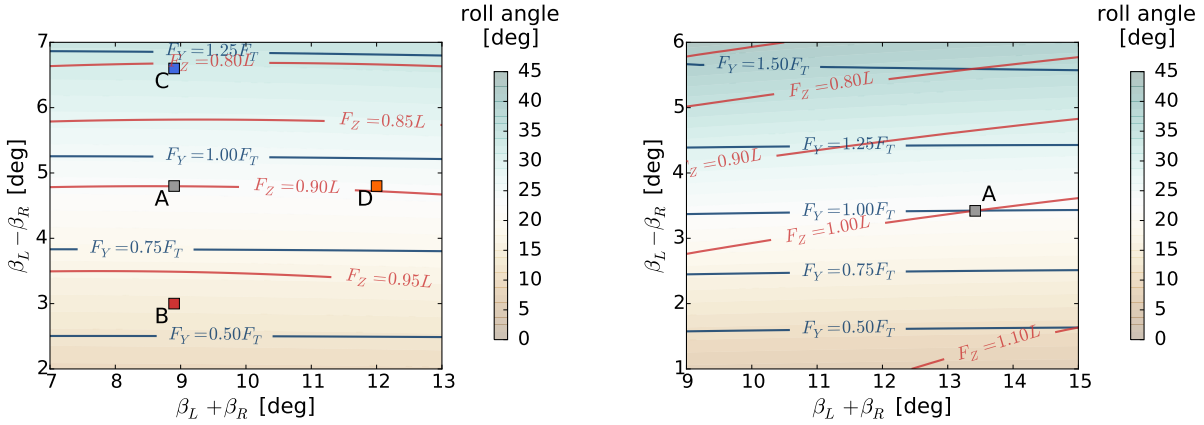
other.

In both Fig. 20a and 20b the contour lines of the lateral force, $F_Y$, are roughly parallel to the $\beta_L - \beta_R$ isolines, as roll attitude and lateral force are correlated. For the $\sigma = 1.1$ wing, however, also the lines of constant vertical force, $F_Z$, are aligned along the same direction. Starting from point $A$, therefore, a change in roll attitude (i.e. of $\beta_L - \beta_R$) always leads to a decrease in either lateral (point $B$) or vertical (point $C$) force (see also Fig. 21a and 21b). On the other hand, increasing the overall load acting on the wing by deflecting the ailerons further down is also counter-productive (point $D$) and an even larger effective dihedral is produced, such that the small lift gain on the right wing is cancelled by the reduction of vertical force on the left wing (Fig. 21c). It is interesting to underlining the similitude between this aeroelastic effects and that of ailerons reversal: in the first case, in fact, a deflection of the control surfaces produces unfavourable bending, while in the second one adverse twist. Bending-induced static instabilities have also been reported, with respect to the forward-flight speed, on very flexible flying wings.[36]

As it has been seen, for very low wing flexibility deflecting the control surfaces produces an excessively large effective dihedral. Furthermore, lift increases are limited by the adverse twist occurring along the wing span. A slightly higher wing stiffness ($\sigma = 1.5$), instead, allows to exploit the ailerons for compensating the lift gap: in Fig. 20b, in fact, the vertical force, $F_Z$, always increases with $\beta_L + \beta_R$ and, as expected, the steady state aileron commands predicted via single-shooting (see also the time histories in Fig. 18a) correspond to the intersection between the $F_Y = F_T$ and $F_Z = L$ lines (point $A$ in Fig. 20b). There is a minimum level of bending stiffness to achieve a desired steady-state manoeuvre on a very flexible vehicle.

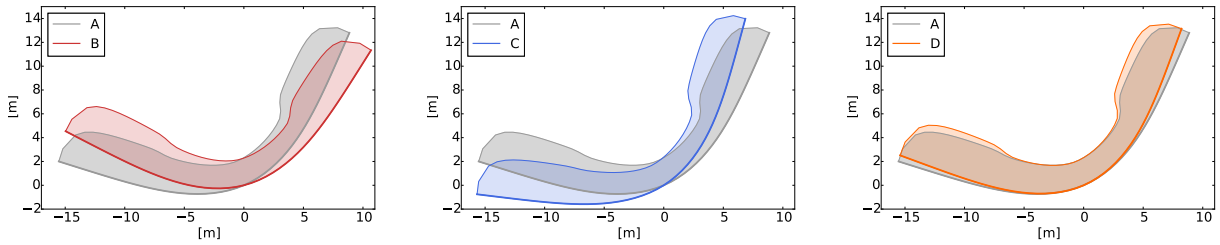
## V. Conclusions

A methodology to identify optimal manoeuvres with very flexible wings has been proposed. A full aeroelastic model — based here on the coupling of composite beams and unsteady vortex lattices — is first needed that captures geometrical-nonlinear effects on both the structure and the aerodynamics. Embedding this into an optimal control framework allows to obtain the control inputs time-histories required to perform a desired manoeuvre from an optimisation problem. In addition, a elastified flight-dynamics model (EFDM), based on aeroelastic corrections of the stability derivatives has also been developed and assessed for this task. It has been seen to capture the relevant physics for slow enough manouvres while simplifying considerably the description of the roll dynamics. In the EFDM, the aileron input for a given manoeuvre can be identified by inspection, hence providing a term of comparison to assess the single-shooting based methodology. As expected, this approach was seen to perform well for relatively rigid wings and for relatively slow actuations.




(a) $\sigma = 1.1$ (b) $\sigma = 1.5$

Figure 20: Visualisation of the roll attitude and isolines of the lateral and vertical forces produced at the steady state by a $\sigma = 1.1$ and a $\sigma = 1.5$ wing for different aileron deflections $(\beta_L, \beta_R)$. Points A, B, C and D correspond to representative configurations.




(a) A vs. B (b) A vs. C (c) A vs. D

Figure 21: Comparison of the aerodynamic loads and wing deformed configuration of representative points of the space $(\beta_L, \beta_R)$ shown in Fig. 20a.

It also provides an initial guess for the optimization on the full problem.

The key features of the rolling dynamics of very flexible wings have been investigated. Firstly, adverse twist deformations — which are a linear aeroelastic effect — appear as the ailerons deflect, thus reducing the control authority. In addition to that, the wing dihedral associated to bending, as well as the asymmetric displacements between starboard and port wing, produce geometrical nonlinearities that diminish the damping associated to the roll rate while increasing the wing stability. Structural vibrations were also found to be asymmetric, being these more intense on the wing where larger bending would occur.

Using the single-shooting method, the trade-off between a number of performance indices associated to the wing roll dynamics can be investigated. This has been made possible here by identifying the manoeuvre in a multi-objective optimisation problem. Dividing the manoeuvre into segments allows to compromise a fast

wing response with a low level of subsequent structural vibrations (although not necessarily during the initial transient dynamics, where they can contribute to increase performance). Moreover, independent ailerons deflections have been exploited to define unconventional manoeuvre objectives. These investigations also pointed out specific handling quality limitations of very flexible wings, which could otherwise be identified only through an extensive sampling of different actuation scheduling strategies.

In summary, this work shows that the optimal control approach, based upon a nonlinear description of flexible vehicle dynamics, can explore unconventional actuation strategies and exploit specific features of a given vehicle to obtain trade-offs between different performance indices associated to a manoeuvre. The current formulation has dealt with constrained vehicle kinematics with a limited number of actuators and, for larger problems, it would require the development of a more computationally-efficient (e.g., adjoint-based) sensitivity analysis. Through this relatively simple example, it has been shown that the approach provides a valuable alternative not only for exploring novel actuation strategies, but also to assess and quantify the limit performance of light and very flexible wings.

## Acknowledgements

This research was made possible in part by Doctoral Training Partnership funds of the UK Engineering and Physical Science Research Council (EPSRC). All results in this paper are available as open data. Information on access can be found at `http://www.imperial.ac.uk/aeroelastics/software`.

## References

[1] Pendleton, E. W., Bessette, D., Field, P. B., Miller, G. D., and Griffin, K. E., "Active Aeroelastic Wing Flight Research Program: Technical Program and Model Analytical Development," *Journal of Aircraft*, Vol. 37, No. 4, 2000, pp. 554–561.

[2] Lind, R. and Brenner, M., *Robust Aeroservoelastic Stability Analysis*, Advances in Industrial Control, Springer, London, 2012.

[3] Cesnik, C. E., Palacios, R., and Reichenbach, E. Y., "Reexamined Structural Design Procedures for Very Flexible Aircraft," *Journal of Aircraft*, Vol. 51, No. 5, 2014, pp. 1580–1591.

[4] Winther, B. A., Goggin, P. J., and Dykman, J. R., "Reduced-Order Dynamic Aeroelastic Model De-

velopment and Integration with Nonlinear Simulation," *Journal of Aircraft*, Vol. 37, No. 5, sep 2000, pp. 833–839.

[5] Mukhopadhyay, V., "Historical Perspective on Analysis and Control of Aeroelastic Responses," *Journal of Guidance, Control, and Dynamics*, Vol. 26, No. 5, 2003, pp. 673–684.

[6] Meirovitch, L. and Tuzcu, I., "Unified Theory for the Dynamics and Control of Maneuvering Flexible Aircraft," *AIAA Journal*, Vol. 42, No. 4, 2004, pp. 714–727.

[7] Baldelli, D. H., Chen, P. C., and Panza, J., "Unified Aeroelastic and Flight Dynamic Formulation via Rational Function Approximations," *Journal of Aircraft*, Vol. 43, No. 3, 2006, pp. 763–772.

[8] Hesse, H. and Palacios, R., "Reduced-Order Aeroelastic Models for Dynamics of Maneuvering Flexible Aircraft," *AIAA Journal*, Vol. 52, 2014, pp. 1–16.

[9] Patil, M. J. and Hodges, D. H., "Output Feedback Control of the Nonlinear Aeroelastic Response of a Slender Wing," *Journal of Guidance, Control, and Dynamics*, Vol. 25, No. 2, 2002, pp. 302–308.

[10] Tuzcu, I., Marzocca, P., Cestino, E., Romeo, G., and Frulla, G., "Stability and Control of a High-Altitude, Long-Endurance UAV," *Journal of Guidance, Control, and Dynamics*, Vol. 30, No. 3, 2007, pp. 713–721.

[11] Patil, M. J. and Hodges, D. H., "Flight Dynamics of Highly Flexible Aircraft," *Journal of Aircraft*, Vol. 45, No. 2, 2008, pp. 538–545.

[12] Shearer, C. M. and Cesnik, C. E., "Nonlinear Flight Dynamics of Very Flexible Aircraft," *Journal of Aircraft*, Vol. 44, No. 5, 2007, pp. 1528–1545.

[13] Palacios, R., Murua, J., and Cook, R. G., "Structural and Aerodynamic Models in Nonlinear Flight Dynamics of Very Flexible Aircraft," Vol. 48, No. 11, 2010, pp. 2648–2659.

[14] Shearer, C. M. and S. Cesnik, C. E., "Trajectory Control for Very Flexible Aircraft," *Journal of Guidance, Control, and Dynamics*, Vol. 31, No. 2, 2008, pp. 340–357.

[15] Cook, R. G., Palacios, R., and Goulart, P. J., "Robust Gust Alleviation and Stabilization of Very Flexible Aircraft," *AIAA Journal*, Vol. 51, No. 2, 2013, pp. 330–340.

[16] Wang, Y., Wynn, A., and Palacios, R., "Nonlinear Modal Aeroservoelastic Analysis Framework for Flexible Aircraft," *AIAA Journal*, Vol. 54, No. 10, 2016, pp. 3075–3090.

[17] Allison, J. and Herber, D. R., "Multidisciplinary Design Optimization of Dynamic Engineering Systems," *AIAA Journal*, Vol. 52, No. 4, 2014, pp. 691–710.

[18] Martins, J. R. R. A. and Lambe, A. B., "Multidisciplinary Design Optimization: A Survey of Architectures," *AIAA Journal*, Vol. 51, No. 9, 2013, pp. 2049–2075.

[19] Maraniello, S. and Palacios, R., "Optimal Vibration Control and Co-Design of Very Flexible Actuated Structures," *Journal of Sound and Vibration*, Vol. 377, 2016, pp. 1–21.

[20] Hodges, D. H., "A Mixed Variational Formulation Based on Exact Intrinsic Equations for Dynamics of Moving Beams," *International Journal of Solids and Structures*, Vol. 26, No. 11, 1990, pp. 1253–1273.

[21] Hesse, H. and Palacios, R., "Consistent structural linearisation in flexible-body dynamics with large rigid-body motion," *Computers & Structures*, Vol. 110–111, 2012, pp. 1–14.

[22] Murua, J., Palacios, R., and Graham, J. M. R., "Applications of the Unsteady Vortex-Lattice Method in Aircraft Aeroelasticity and Flight Dynamics," *Progress in Aerospace Sciences*, Vol. 55, 2012, pp. 46–72.

[23] Simpson, R. J. S., Palacios, R., and Murua, J., "Induced-Drag Calculations in the Unsteady Vortex Lattice Method," *AIAA Journal*, Vol. 51, No. 7, 2013, pp. 1775–1779.

[24] Khot, N. S., Eastep, F. E., and Kolonay, R. M., "Method for Enhancement of the Rolling Maneuver of a Flexible Wing," *Journal of Aircraft*, Vol. 34, No. 5, 1997, pp. 673–678.

[25] Murua, J., Hesse, H., Palacios, R., and Graham, J. M. R., "Stability and Open-Loop Dynamics of Very Flexible Aircraft Including Free-Wake Effects," *52nd AIAA/ASME/ASCE/AHS/ASC Structures, Structural Dynamics and Materials Conference*, Denver, Colorado, 2011.

[26] Hesse, H., Palacios, R., and Murua, J., "Consistent Structural Linearization in Flexible Aircraft Dynamics with Large Rigid-Body Motion," *AIAA Journal*, Vol. 52, No. 3, 2014, pp. 528–538.

[27] Lin, Q., Loxton, R., and Teo, K. L., "The Control Parameterization Method for Nonlinear Optimal Control: A Survey," *Journal of Industrial and Management Optimization*, Vol. 10, No. 1, 2013, pp. 275–309.

[28] Schlegel, M., Stockmann, K., Binder, T., and Marquardt, W., "Dynamic Optimization Using Adaptive Control Vector Parameterization," *Computers & Chemical Engineering*, Vol. 29, No. 8, 2005, pp. 1731–1751.

[29] Fabien, B. C., "Piecewise Polynomial Control Parameterization in the Direct Solution of Optimal Control Problems," *Journal of Dynamic Systems, Measurement, and Control*, Vol. 135, No. 3, 2013.

[30] Kraft, D., "A Software Package for Sequential Quadratic Programming," Tech. rep., DLR German Aerospace Center Institute for Flight Mechanics, Köln, Germany, 1988.

[31] Stevens, B. and Lewis, F., *Aircraft Control and Simulation*, John Wiley & Sons, New York, NY, USA, 1992.

[32] Patil, M. J., Hodges, D. H., and Cesnik, C. E. S., "Nonlinear Aeroelasticity and Flight Dynamics of High-Altitude Long-Endurance Aircraft," *Journal of Aircraft*, Vol. 38, No. 1, 2001, pp. 88–94.

[33] Peters, D. A. and Cao, W.-M., "Finite State Induced Flow Models Part I: Two-Dimensional Thin Airfoil," *Journal of Aircraft*, Vol. 32, No. 2, 1995, pp. 313–322.

[34] Patil, M. J. and Hodges, D. H., "On the Importance of Aerodynamic and Structural Geometrical Nonlinearities in Aeroelastic Behavior of High-Aspect-Ratio Wings," *Journal of Fluids and Structures*, Vol. 19, 2004, pp. 905–915.

[35] Tang, D. M. and Dowell, E. H., "Effects of Geometric Structural Nonlinearity on Flutter and Limit Cycle Oscillations of High-Aspect-Ratio Wings," *Journal of Fluids and Structures*, Vol. 19, 2004, pp. 291–306.

[36] Patil, M. J. and Hodges, D. H., "Flight Dynamics of Highly Flexible Flying Wings," *Journal of Aircraft*, Vol. 43, No. 6, 2006, pp. 1790–1798.